THE JOURNAL OF BIOLOGICAL CHEMISTRY VOL. 283, NO. 28, pp. 19422–19431, July 11, 2008

Interaction and Stoichiometry of the Peripheral Stalk Subunits NtpE and NtpF and the N-terminal Hydrophilic Domain of NtpI of *Enterococcus hirae* V-ATPase*

Received for publication, March 5, 2008, and in revised form, May 2, 2008 Published, JBC Papers in Press, May 6, 2008, DOI 10.1074/jbc.M801772200

Misaki Yamamoto,[a,b] Satoru Unzai,[c] Shinya Saijo,[d] Kazuki Ito,[e] Kenji Mizutani,[f] Chiyo Suno-Ikeda,[g] Yukako Yabuki-Miyata,[b] Takaho Terada,[b] Mitsutoshi Toyama,[b] Mikako Shirouzu,[b] Takuya Kobayashi,[f,g] Yoshimi Kakinuma,[h] Ichiro Yamato,[a] Shigeyuki Yokoyama,[b,i] So Iwata,[b,f,g] and Takeshi Murata[b,f,g1]

From the [a]Department of Biological Science and Technology, Tokyo University of Science, 2641 Yamazaki, Noda-shi, Chiba 278-8510, the [b]Protein Research Group, RIKEN Genomic Sciences Center, 1-7-22 Suehiro-cho, Tsurumi, Yokohama 230-0045, the [c]Protein Design Laboratory, Yokohama City University, 1-7-29 Suehiro-cho, Tsurumi, Yokohama 230-0045, the [d]Research and Utilization Division, Japan Synchrotron Radiation Research Institute, SPring-8, 1-1-1 Kouto, Sayo-cho, Sayo-gun, Hyogo 679-5198, the [e]Structural Materials Science Laboratory, RIKEN SPring-8 Center, 1-1-1 Kouto, Sayo-cho, Sayo-gun, Hyogo 679-5148, the [f]Department of Cell Biology, Faculty of Medicine, Kyoto University, Yoshidakonoe-cho, Sakyo-ku, Kyoto 606-8501, the [g]Iwata Human Receptor Crystallography Project, Japan Science and Technology Agency, ERATO, Yoshidakonoe-cho, Sakyo-ku, Kyoto 606-8501, the [h]Laboratory of Molecular Physiology and Genetics, Faculty of Agriculture, Ehime University, 3-5-7 Tarumi, Matsuyama, Ehime 790-8566, and the [i]Department of Biophysics and Biochemistry, Graduate School of Science, The University of Tokyo, 7-3-1 Hongo, Bunkyo-ku, Tokyo 113-0033, Japan

The vacuolar ATPase (V-ATPase) is composed of a soluble catalytic domain and an integral membrane domain connected by a central stalk and a few peripheral stalks. The number and arrangement of the peripheral stalk subunits remain controversial. The peripheral stalk of Na^+-translocating V-ATPase from *Enterococcus hirae* is likely to be composed of NtpE and NtpF (corresponding to subunit G of eukaryotic V-ATPase) subunits together with the N-terminal hydrophilic domain of NtpI (corresponding to subunit a of eukaryotic V-ATPase). Here we purified NtpE, NtpF, and the N-terminal hydrophilic domain of NtpI ($NtpI^{Nterm}$) as separate recombinant His-tagged proteins and examined interactions between these three subunits by pulldown assay using one tagged subunit, CD spectroscopy, surface plasmon resonance, and analytical ultracentrifugation. $NtpI^{Nterm}$ directly bound NtpF, but not NtpE. NtpE bound NtpF tightly. $NtpI^{Nterm}$ bound the NtpE-F complex stronger than NtpF only, suggesting that NtpE increases the binding affinity between $NtpI^{Nterm}$ and NtpF. Purified NtpE-F-I^{Nterm} complex appeared to be monodisperse, and the molecular masses estimated from analytical ultracentrifugation and small-angle x-ray scattering (SAXS) indicated that the ternary complex is formed with a 1:1:1 stoichiometry. A low resolution structure model of the complex produced from the SAXS data showed an elongated "L" shape.

The vacuolar ATPases (V-ATPases)[2] function as ATP-dependent proton pumps in the membranes of acidic organelles and in plasma membranes of eukaryotic cells. This acidification is involved in concentration of neurotransmitters, processing of secretory proteins, endocytosis, and other important cellular processes (1). The V-ATPase contains a globular catalytic domain, V_1, which hydrolyzes ATP, attached by central and peripheral stalks to an integral membrane domain, V_o, which pumps ions across the membrane. ATP hydrolysis generates rotation of the central stalk and an attached membrane ring of hydrophobic subunits. Ions are pumped through a pathway at the interface between the rotating ring and a static membrane component, which is linked to the outside of the V_1 domain by the peripheral stalk (1).

In yeast, the V_1 domain contains subunits A–H, while the membrane-bound V_o is made of subunit a, c, c′, c″, d, and e. The core of the V_1 domain is composed of a hexameric arrangement of alternating A and B subunits responsible for ATP binding and hydrolysis. The V_o domain consists of a ring of proteolipid subunits (c, c′, and c″) adjacent to subunits a and e. The V_1 and V_o domains are connected by a central stalk, composed of subunits D and F of V_1 and subunit d of V_o, and a few peripheral stalks, composed of subunits C, E, G, and H together with N-terminal domain of subunit a (1). Because V-ATPases function in various physiological processes, regulation of their activity is very important. The peripheral stalk subunits have been shown to play an important role in the regulation of the enzyme via a reversible dissociation and re-association mechanism (2, 3). To understand the structural mechanism of the regulation, information on the stoichiometry of the subunits comprising

* This work was supported by grants-in-aid 19042022 and 18770122 (to T. M.) from the Ministry of Education, Culture, Sports, Science and Technology of Japan (MEXT), by the RIKEN Structural Genomics/Proteomics Initiative, the National Project on Protein Structural and Functional Analysis from MEXT, and by Targeted Proteins Research Program (B-37) from MEXT. The costs of publication of this article were defrayed in part by the payment of page charges. This article must therefore be hereby marked "*advertisement*" in accordance with 18 U.S.C. Section 1734 solely to indicate this fact.

[1] To whom correspondence should be addressed: Dept. of Cell Biology, Faculty of Medicine, Kyoto University, Yoshidakonoe-cho, Sakyo-ku, Kyoto 606-8501, Japan. Tel.: 81-75-753-4375; Fax: 81-75-753-4660; E-mail: t.murata@mfour.med.kyoto-u.ac.jp.

[2] The abbreviations used are: V-ATPase, vacuolar ATPase; $NtpI^{Nterm}$, N-terminal domain of NtpI subunit; SAXS, small-angle X-ray scattering; AUC, analytical ultracentrifugation; AUC/SE, analytical ultracentrifugation sedimentation equilibrium; AUC/SV, analytical ultracentrifuge sedimentation velocity; R_{eq}, equilibrium resonance units; NSD, normalized spatial discrepancy; Nterm, N-terminal.

the peripheral stalk and the nature of their interaction is essential. Interactions within the V_1 domain, between subunits E, G, and C (4), H and a (5), a and C (6), a and G (7), and E and G (8) have been demonstrated by cross-linking studies and/or *in vitro* pulldown techniques. Electron microscopic studies have indicated that subunits E and G formed a rod-shaped heterodimer (8, 9) and are both present in two or three copies per complex (10–12). These findings suggest that the peripheral stalk of V-ATPase is composed of two or three EG heterodimers together with subunits H and C, and the N-terminal domain of subunit a. However, the precise subunit arrangement in the stalk regions remains controversial.

V-ATPases are also found in bacteria (13–15). We have identified a variant of V-ATPase in a fermentative bacterium *Enterococcus hirae*, which physiologically transports Na^+ rather than H^+ (16–18). The enzyme is encoded by nine *ntp* subunit genes (*ntpFIKECGABD*) organized in the *ntp* operon (19, 20). Amino acid sequences of NtpF, -I, -K, -E, -C, -G, -A, -B, and -D are homologous to those of subunits G, a, c, E, d, F, A, B, and D of eukaryotic V-ATPases, respectively (21). Bacterial V-ATPases have no counterpart for subunit C and H of eukaryotic V-ATPases that are responsible for modulating the interaction between V_1 and V_o (22). Therefore, *E. hirae* Na^+-ATPase is a homolog of eukaryotic V-ATPase, with a simpler subunit composition. The V_1 domain responsible for ATP-driven rotation is composed of the Ntp-A, -B, -C(d), -D, -E -F(G), and -G(F) subunits. The V_o domain responsible for utilization of the rotation energy of V_1 for Na^+ translocation is composed of oligomers of the 16-kDa NtpK(c) forming a membrane rotor ring and a single copy of the NtpI(a) subunit (Fig. 1). The peripheral stalk of this enzyme is likely to be composed of NtpF(G) and NtpE with the N-terminal domain of NtpI(a) (Fig. 1, shown in *gray*), although the subunit arrangement and stoichiometry of these subunits are unclear.

In this study, NtpE, NtpF, and the N-terminal hydrophilic domain of NtpI ($NtpI^{Nterm}$) were individually purified, and the interactions between the three subunits were investigated. The purified $NtpI^{Nterm}$ was shown to bind directly to NtpF but not NtpE, and the three subunits make up the ternary complex with a 1:1:1 stoichiometry. A low resolution structure model of the complex obtained by SAXS reveals an elongated "L"-shape.

EXPERIMENTAL PROCEDURES

Initial Expression Trials of NtpE, NtpF, and $NtpI^{Nterm}$—Full-length *ntpE* and *ntpF* genes, and nine DNA constructs encoding the N-terminal soluble domain of NtpI with different C-terminal boundaries were amplified by PCR. The amplified DNA fragments were incorporated by overlap PCR to the T7 promoter sequence, the ribosome-binding site, the His tag, the cleavage site for tobacco etch virus protease, a linker sequence, and the T7 terminator sequence, which are coding following protein sequence from N terminus: His tag (His-7)/tobacco etch virus cleavage site (EHLYFQG)/linker (SSGSSG)/protein sequence (23). The His-tagged proteins were synthesized by the dialysis mode of cell-free protein expression using these PCR DNA templates, as described elsewhere (24). The total reaction mixtures were centrifuged to remove insoluble proteins, and the total and soluble fractions were subjected to SDS-PAGE to assess the quantity and the solubility of the expressed proteins.

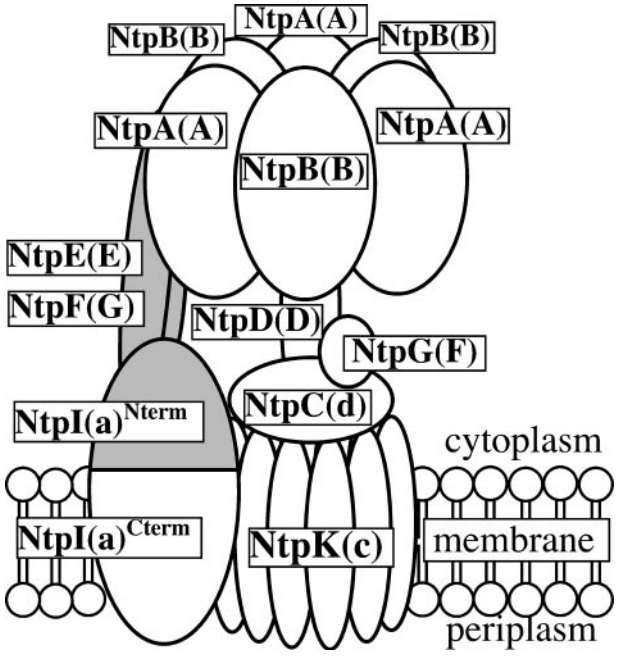

FIGURE 1. **Structural model of V-ATPase from *E. hirae*.** In this study, NtpE, NtpF, and $NtpI^{Nterm}$ shown in *gray* were examined. *Letters in parentheses* indicate the names of the corresponding subunits of eukaryotic V-ATPase.

Expression and Purification of the Subunits—The DNA fragments expressed in the cell-free system were cloned into the plasmid vector, pET23d, and expressed in *Escherichia coli* BL21(DE3) by isopropyl (thio)-β-D-galactoside induction. The *E. coli* lysate was loaded onto a HisTrap HP column (GE Healthcare, England) equilibrated with A buffer (50 mM Tris-HCl, 750 mM NaCl, 5 mM 2-mercaptoethanol, and 10 mM imidazole, pH 8.0), and bound proteins were eluted with B buffer (50 mM Tris-HCl, 300 mM NaCl, 5 mM 2-mercaptoethanol, and 500 mM imidazole, pH 8.0). The sample buffer was exchanged to A buffer using a HiPrep 26/10 desalting column. To obtain non-tagged protein, the proteins were treated with tobacco etch virus protease at 4 °C for 12 h. The reaction solution was loaded onto a HisTrap HP column again, and the flow-through fractions containing the non-tagged proteins were pooled. This step was not included in protocol for the purification of His-tagged proteins. The protein samples were then dialyzed against C buffer (50 mM Tris-HCl, 10 mM NaCl, 5 mM 2-mercaptoethanol, pH 8.5), loaded onto a HiTrap Q HP (GE Healthcare, England) column equilibrated with C buffer and eluted with a linear gradient of 10 mM-1.0 M NaCl. Finally, the samples were loaded onto a HiLoad 16/60 Superdex 200pg (GE Healthcare) column equilibrated with D buffer (50 mM Tris-HCl, 100 mM NaCl, 10% glycerol, 1 mM dithiothreitol, pH 7.5) and eluted using D buffer. The purified sample was concentrated by ultrafiltration (YM 10 filter, Amicon).

Pulldown Assay Using Only One Tagged Subunit and Co-purification of the Complex—His-tagged sample (NtpE or $NtpI^{Nterm}$) and an excess of non-tagged sample(s) (NtpE, NtpF, and/or $NtpI^{Nterm}$) were mixed and incubated for 90 min on ice. The mixture was loaded on a HisTrap HP column equilibrated

with A buffer, the column was washed with 5 column volumes of A buffer, and bound proteins were eluted with B buffer. All eluted proteins were analyzed by SDS-PAGE. To obtain non-tagged complex (NtpE-F or NtpE-F-I^{Nterm}), the histidine-affinity tag was removed by tobacco etch virus protease treatment at 4 °C for 12 h. The reaction solution was loaded onto a HisTrap HP column again, and the flow-through fraction was pooled. Finally, concentrated pooled samples were loaded onto a HiLoad 16/60 Superdex 200pg (GE Healthcare) column equilibrated with D buffer and eluted with D buffer. Purified complex was concentrated by ultrafiltration (YM10 filter).

Measurements of CD Spectroscopy—The CD spectroscopy was performed with a Jasco J-725 spectropolarimeter (Jasco, Japan). The purified subunits and complexes were dialyzed in phosphate-buffered saline (pH 7.4), and diluted to 0.25 mg of protein/ml which were determined using the BCA Protein Assay Kit (Pierce) using bovine serum albumin as the standard. Far UV scans were collected between 200 nm and 240 nm in 0.2 nm steps at 20 °C. All CD measurements were corrected for background buffer contribution. The raw data were converted to molar residual ellipticity (θ) using standard analysis.

Real-time Binding Assay by Surface Plasmon Resonance—The BIAcore 3000 system and reagents, including sensor chips and the amine coupling kit, were obtained from GE Healthcare. Purified NtpE (50 μg/ml) or $NtpI^{Nterm}$ (30 μg/ml) in 10 mM sodium acetate (pH 4.5) was immobilized on a CM5 sensor chip using an amine coupling kit according to the manufacturer's instructions. Purified sample was passed over the surface of the sensor chip with a typical flow rate of 30 μl/min, and the interactions were monitored for 3 min at 20 °C. The sensor surface was then washed with D buffer containing 2% glycerol for 3 min. Chip regeneration conditions varied according to the interactions studied: for NtpE (ligand)-NtpF (analyte) interaction, the chip was washed with 10 mM glycine (pH 1.5) for 30 s; for $NtpI^{Nterm}$ (ligand)-NtpF (analyte) interaction and $NtpI^{Nterm}$ (ligand)-NtpEF complex (analyte) interaction, the chip was washed with D buffer containing 2% glycerol for 5 min, which is enough to dissociate the bound analyte. For high affinity interactions of the NtpE-NtpF and $NtpI^{Nterm}$-NtpEF complexes, the association and dissociation rate constants (k_{on} and k_{off}) were calculated using BIAevaluation software (Version 4.1, GE Healthcare) with the program, 1:1 (Langmuir) binding model. The dissociation constant (K_D) was determined from the k_{off}/k_{on} values. In the case of the $NtpI^{Nterm}$-NtpF interaction, it was not possible to evaluate the rate constants from the k_{off}/k_{on} values because of low affinity. We obtained an approximate equilibrium dissociation constant (K_D) by measuring the equilibrium resonance units (R_{eq}) at several analyte concentrations at equilibrium. The fitted curve (R_{eq} *versus* concentrations of analyte) and the K_D values were obtained using the BIAevaluation software with a single 1:1 interaction binding isotherm.

Analytical Ultracentrifugation—Sedimentation velocity (AUC/SV) and equilibrium (AUC/SE) experiments were carried out using an Optimal XL-1 analytical ultracentrifuge (Beckman Coulter). For AUC/SV experiments, cells with a standard Epon two-channel centerpiece and sapphire windows were used. Samples in D buffer and reference buffer (D buffer) were loaded into cells. The rotor temperature was equilibrated at 20 °C in the vacuum chamber for 1–2 h prior to start-up. Absorbance (A_{280}) scans were collected at 10-min intervals during sedimentation at 50×10^3 rpm. The sample concentrations were 0.8, 0.4, and 0.2 mg of protein/ml protein for purified subunits (NtpE, NtpF, and $NtpI^{Nterm}$) or 0.8 mg of protein/ml proteins for mixed samples and the purified complex (NtpE-F-I^{Nterm}). Partial specific volume of the protein, solvent density, and solvent viscosity were calculated from standard tables using the program SEDNTERP, version 1.09 (25). The resulting scans were analyzed using the continuous distribution (c(s)) analysis module in the program Sedfit version 11.0 (26). In this analysis a differential sedimentation coefficient distribution, c(s), that deconvolutes diffusion effects, based on the direct boundary modeling with distributions of Lamm equation solutions, is determined (27). Sedimentation coefficient increments of 200 were used in the appropriate range for each sample, and the weight average frictional ratio (f/f_o) was allowed to float during fitting. The weight average sedimentation coefficient was obtained by integrating the range of sedimentation coefficients in which peaks were present. The $s_{20,w}$ value, sedimentation coefficient corrected to 20 °C in pure water, was calculated from the observed sedimentation coefficient value using the program SEDNTERP.

AUC/SE experiments were also carried out in cells with a six-channel centerpiece and quartz windows. The samples were diluted 0.4, 0.2, and 0.15 mg of protein/ml with D buffer. The absorbance wavelength was set at 280 nm, and data were acquired at 20 °C. Data were obtained at 12, 15, and 18×10^3 rpm for NtpE and NtpF, at 9, 12, and 15×10^3 rpm for $NtpI^{Nterm}$, at 7, 10, and 13×10^3 rpm for mixed samples, and at 6, 9, and 12×10^3 rpm for purified NtpE-F-I^{Nterm} complex. A total equilibration time of 16 h was used for each speed, with a scan taken at 12 h and 14 h to ensure equilibrium had been reached. The optical baseline was determined by accelerating at 40×10^3 rpm at the end of data collection. Data analysis was performed by global analysis of data sets obtained at different loading concentrations and rotor speeds using UltraSpin software (MRC Center for Protein Engineering, Cambridge, UK, www.mrc-cpe.cam.ac.uk/ultraspin).

SAXS—SAXS experiments were carried out at the RIKEN Structural Biology Beamline I BL45XU at SPring-8, Japan (28). The x-ray wavelength used, λ, was 0.09 nm, and the beam size at the sample position was 0.25×0.5 mm^2. The sample-to-detector distance was determined to be 3343 mm by the silver behenate ($d = 5.380$ nm, The Gem Dagout) as a standard sample in the SAXS experiment. This setup covers the momentum transfer ranges $0.057\ \text{nm}^{-1} < q < 2.133\ \text{nm}^{-1}$ (where $q = 4\pi \sin\theta/\lambda$, 2θ is the scattering angle), however, the data points were discarded in $q < 0.1\ \text{nm}^{-1}$ to avoid the influence of parasitic scattering into the result. The sample temperature was controlled to 293.00 ± 0.01 K with a high precision thermoelectric controller. The sample solutions were brought into a sample cell, which has 30 μl in volume, a path length of 3 mm, and a pair of 0.02-mm thickness synthetic quartz windows. The SAXS patterns of protein solutions and corresponding buffer were measured by an on-line imaging plate detector, Rigaku R-AXIS IV++. The sample cell was continuously moved during x-ray exposure to reduce the radiation damage. The SAXS

profiles were collected as three subsequent exposures of 100 s with the attenuated beam (~1/100 against the intrinsic intensity). The radiation damage was tested by comparing subsequent exposures of the same sample, and only the data without the signs of radiation damage were analyzed. Exposures from sample and buffer were alternated to minimize the possible effects of drift in any experimental parameters. The SAXS patterns were circularly averaged and reduced to one-dimensional profiles using the in-house software (28). Those scattering profiles were then normalized by the x-ray intensity measured by the ionization chamber placed upstream of the sample, the exposure time, and the protein concentration c (mg/ml) of the solution. Data processing was performed using the program PRIMUS in the software package of ATSAS 2.2 (Svergun). These data treatments resulted in scattering profiles, $I(q)$. To eliminate inter-particle interference, $I(q)$, recorded at three different protein concentrations (1.7, 2.4, and 3.0 mg of protein/ml) as described above, were scaled using a protein concentration c,

$$I(q, c) = I(q)/c \quad \text{(Eq. 1)}$$

where $I(q, c)$ denotes the SAXS profile normalized by weight percent concentration. The radius of gyration was determined by fitting the innermost portion of $I(q, c)$ to,

$$I(q, c) = I(0, c)\ \exp(-R_g(c)^2q^2/3) \quad \text{(Eq. 2)}$$

where $I(0, c)$ and $R_g(c)$ are the concentration-normalized intensity at an angle of zero ($q = 0$) and the apparent radius of gyration at the protein concentration c, respectively. The value of $R_g(c)$ was determined using Guinier approximation with $q_{max}R_g(c) < 1.3$. Data points for $q < 0.143$ nm^{-1}, which were affected by intermolecular interactions, were excluded from the data fit. The reported SAXS data were treated as monodisperse systems unless otherwise mentioned. The molecular mass of protein, M_w, was estimated by comparing the extrapolated forward scattering intensity, $I(0, c)$: $c \to 0$, of NtpE-F-I^{Nterm} complex with that of bovine serum albumin (Sigma-Aldrich) as the standard protein in SAXS measurements. Bovine serum albumin protein is a 66.4-kDa monomeric protein, which is one of the most common standards for estimating the molecular mass by using SAXS. The pair distribution function, $P(r)$, was calculated by the program GNOM (29) based on an indirect Fourier transform algorithm in the q range from 0.1072 to 2.133 nm^{-1} for NtpE-F-I^{Nterm} complex. The maximum molecular length, D_{max}, was estimated as a distance, r, where $P(r) = 0$ for $r \geq D_{max}$.

Low Resolution Shape Reconstruction—After processing the scattering data with GNOM, low resolution shape reconstruction of the NtpE-F-I^{Nterm} complex was conducted with an *ab initio* bead-modeling program, DAMMIN (30). DAMMIN were applied to SAXS profiles in $q < 2.133$ nm^{-1} and to those weighted by q^{-4} to ensure Porod's law. Reproducibility of the structural solution was confirmed by repeating ten reconstructions without any shape and symmetrical constraints. To evaluate the creditability and accuracy of the reconstructed model, we employed the program, DAMAVER (31), which aligns all reconstructed models and removes outliers below a given cut-off volume, for setting up the criterion of the pairwise normalized spatial discrepancies (NSD). The *ab initio* model exceeding ⟨NSD⟩ (mean value of all pairs NSD) + 2δ (NSD) (variation of NSD) were discarded. The most probable model of NtpE-F-I^{Nterm} complex after DAMAVER processing is chosen by the criterion of NSD. The mean value of NSD and variation of NSD in the set of ten *ab initio* models was 0.406 and 0.040, respectively.

TABLE 1
Expression and purification of NtpE, NtpF, and NtpI^{Nterm}

Subunit name	Residues number	Molecular mass[b]	Expression trial[a]		Purification	
			Quantity[c]	Solubility[c]	Stability	Yield[d]
		kDa				
NtpE	1–196	23	++	+++	Stable	3.8
NtpF	1–117	15	+++	+++	Stable	7.8
	1–300	36	+++	−	ND[e]	ND
	1–306	36	+++	−	ND	ND
	1–316	38	+++	−	ND	ND
	1–326	39	+++	+++	ND	ND
NtpI^{Nterm}	1–334	40	+++	+++	ND	ND
	1–341	40	+++	+++	Stable	14.7
	1–355	42	+++	+	Unstable	ND
	1–365	43	+++	+	Unstable	ND
	1–384	46	++	−	ND	ND

[a] +++, very good; ++, good; +, bad; −, very bad.
[b] Theoretical value based on the amino acid sequence without the His tag.
[c] See "Experimental Procedures."
[d] Milligrams of protein/liter culture.
[e] ND, not determined.

Others—Protein concentration was determined using the BCA Protein Assay Kit (Pierce) using bovine serum albumin as the standard. SDS-PAGE was carried out according to Laemmli (32) and stained with Imperial Protein Stain (Pierce). Densitometric analysis of SDS-PAGE gels was performed using ImageJ software (National Institutes of Health). All other chemicals were obtained from Sigma or Wako (Japan). Secondary structure prediction was carried out using the PSIPRED server (available on the World Wide Web).

RESULTS

Expression and Purification of the NtpE, NtpF, and NtpI^{Nterm}—Both NtpE and NtpF expressed as well as soluble His-tagged proteins in the *E. coli* cell-free protein expression system and *in vivo* in *E. coli* BL21 (DE3) cells (Table 1). NtpE and His-tagged NtpE and NtpF were individually purified using column chromatography (see "Experimental Procedures" for details) yielding proteins of apparent molecular masses of 24, 28, and 15 kDa, respectively, as assessed by SDS-PAGE (Fig. 2*A*, *lanes 1–3*).

Subunit NtpI constitutes the membrane-embedded V_o domain together with an NtpK ring, and probably has two half channels for Na^+ translocation across the membrane (33). The 76-kDa NtpI is composed of two regions; a hydrophilic N-terminal half domain, which is likely to form contacts with the peripheral stalk(s), and a hydrophobic C-terminal half domain with several transmembrane helices (predicted as seven by hydropathy analyses) responsible for Na^+ translocation (34). We constructed nine DNA templates, which encode the N-terminal hydrophilic domain of NtpI with different C-terminal boundaries as shown in Table 1. The NtpI^{Nterm} fragment (1–384 residues), which contains the putative first trans-membrane region was expressed as insoluble protein. Shorter

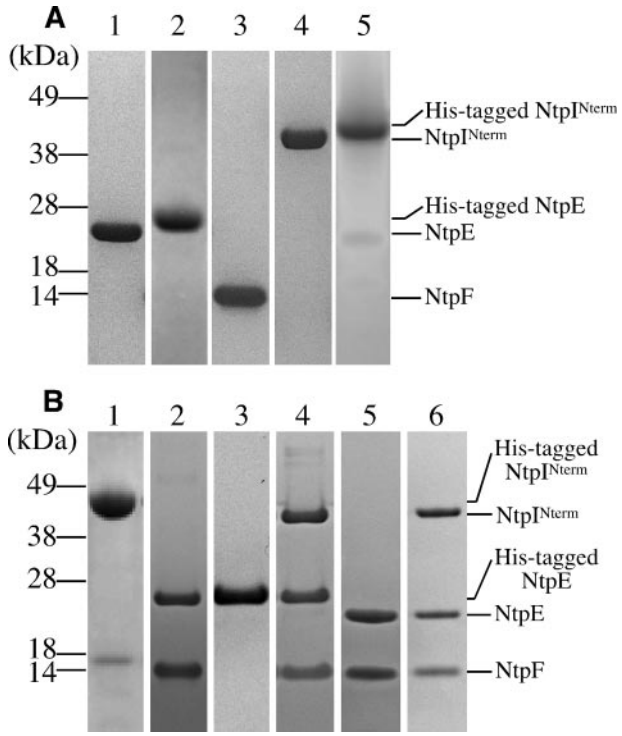

FIGURE 2. **Purification of the subunits and subunit-subunit interaction by pulldown experiment.** *A*, SDS-PAGE analysis of purified subunits. *Lane 1*, NtpE; *lane 2*, His-tagged NtpE; *lane 3*, NtpF; *lane 4*, NtpI^{Nterm}; and *lane 5*, His-tagged NtpI^{Nterm}. *B*, SDS-PAGE analysis of eluted fraction from HisTrap HP column after applying the following mixtures (*lane 1*, His-tagged NtpI^{Nterm} and NtpF; *lane 2*, His-tagged NtpE and NtpF; *lane 3*, His-tagged NtpE and NtpI^{Nterm}; and *lane 4*, His-tagged NtpE, NtpF, and NtpI^{Nterm}), and of purified NtpE-F (*lane 5*) and NtpE-F-I^{Nterm} complexes (*lane 6*).

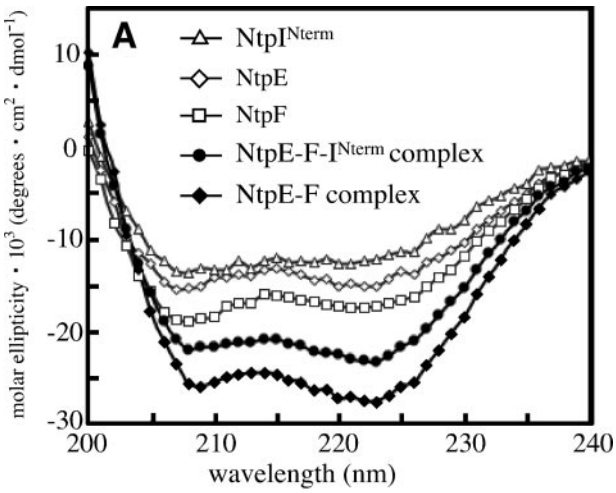

B	a -helix	β-sheet	random coil
NtpE	71%	10%	19%
NtpF	82%	0%	18%
NtpI^{Nterm}	57%	17%	26%
NtpE-F complex	76%	6%	18%
NtpE-F-I^{Nterm} complex	66%	12%	22%

FIGURE 3. **CD spectroscopy of purified subunits and complexes.** *A*, the wavelength dependences of the ellipticities of NtpE (*open diamond*), NtpF (*open square*), NtpI (*open triangle*), NtpE-F complex (*closed diamond*), and NtpE-F-I^{Nterm} complex (*closed circular*) are shown. *B*, the secondary structure composition based on secondary structure prediction using PSIPRED server is listed.

NtpI^{Nterm} fragments (1–365 and 1–355 residues), both of which do not contain the putative trans-membrane region, were expressed as soluble and also as insoluble proteins (Table 1). It was not possible to isolate these proteins, because they aggregated heavily during purification. Other shorter NtpI^{Nterm} fragments (1–341, 1–334, and 1–326 residues) were expressed as all soluble proteins. In this study, we used the NtpI^{Nterm} fragment (1–341), the largest of these three proteins. The remaining shorter NtpI^{Nterm} (1–316, 1–306, and 1–300 residues) were expressed as insoluble proteins (Table 1). It was possible to obtain highly pure non-tagged and His-tagged NtpI^{Nterm} (Fig. 2*A*, *lanes 4* and *5*), with apparent molecular masses of 45 kDa and 47 kDa, respectively, as assessed by SDS-PAGE analysis.

Subunit-Subunit Interactions Assessed by Pulldown Assay and Purification of the NtpE-F and NtpE-F-I^{Nterm} Complexes—The subunit-subunit interactions were examined by pulldown assay using only one tagged subunit by HisTrap HP column chromatography. His-tagged NtpI^{Nterm} bound non-tagged NtpF, although the band of NtpF on SDS-PAGE gel was much weaker than the His-tagged NtpI^{Nterm}; densitometric analysis of the bands stained with Imperial Protein Stain showed that NtpI^{Nterm} and NtpF occur in the molar ratio of 1:0.4 (Fig. 2*B*, *lane 1*). It is possible that non-tagged NtpF bound to His-tagged NtpI^{Nterm} is lost during the HisTrap HP column washing process as the ratio of NtpF to His-tagged NtpI^{Nterm} observed on SDS-PAGE gel changed, depending on the washing time (data not shown). His-tagged NtpE interacted with non-tagged NtpF; densitometric gel analysis showed that the molar ratio of NtpE:NtpF is 1:1.3 (Fig. 2*B*, *lane 2*). Although His-tagged NtpE did not bind NtpI^{Nterm} directly (Fig. 2*B*, *lane 3*), it bound NtpI^{Nterm} complexed with NtpF; densitometric analysis showed that the molar ratio of NtpE:NtpF:NtpI^{Nterm} is 1:1.3:0.8. These findings suggested that NtpE binds NtpF, and NtpF binds NtpI^{Nterm}, directly, and these three subunits form a ternary complex.

The NtpE-F and NtpE-F-I^{Nterm} complexes were purified as described under "Experimental Procedures." SDS-PAGE analysis of the purified NtpE-F complex reveals two bands: NtpE (24 kDa) and NtpF (15 kDa) with a molar ratio of 1:1.3 as estimated by densitometric analysis (Fig. 2*B*, *lane 5*). The purified NtpE-F-I^{Nterm} complex has three bands for NtpI^{Nterm} (45 kDa), NtpE (24 kDa), and NtpF (15 kDa) in SDS-PAGE gel, which were detected with the molar ratio of 1:1.2:1.5 (Fig. 2*B*, *lane 6*).

CD Spectroscopy of Purified Subunits and Complexes—The secondary structure of the purified samples were characterized by far UV CD spectroscopy. Fig. 3*A* shows the wavelength dependences of the ellipticities, which indicated that all the samples contain mainly α-helical structures based on the distinct minima at 222 and 208 nm. The secondary structure composition based on secondary structure prediction using the PSIPRED server is listed in Fig. 3*B*. The predicted α-helix contents of the NtpE (71%) and NtpF (82%) indicate that these subunits are α-helical proteins. The magnitude of the molar ellipticity of the NtpE-F complex at the two minima (222 nm and 208 nm) is greater than those of individual NtpE and NtpF, suggesting that the interaction of NtpE and NtpF leads to an increase in α-helical structure and/or its stabilization. The ratio

of the molar ellipticities at 222 and 208 nm ($\theta_{222}/\theta_{208}$) of NtpE-F complex increased to 1.08 compared with those of NtpE (0.98) and NtpF (0.92). This characteristic increase of the ratio is often observed when two helical elements interact to form higher order structures such as coiled coils (35). Interaction of the corresponding subunits from yeast V-ATPase and *Thermoplasma acidophilum* A-ATPase (resembling V-ATPase structurally) to form a higher order coiled-coil has been previously described (8, 36). NtpI^{Nterm} was predicted to contain a β-sheet of 17% and a random coil of 26% (Fig. 3*B*). Therefore, the magnitude of the molar ellipticity of the NtpE-F-I^{Nterm} complex at the two minima is likely to be smaller than that of NtpE-F complex.

Binding Affinity of the Subunit Interactions Analyzed Using the BIAcore System—We performed surface plasmon resonance analysis to estimate the binding affinities for the subunit interactions detected by pulldown assay as described above; interactions of NtpE-NtpF, NtpI^{Nterm}-NtpF, and NtpI^{Nterm}-NtpEF complex. When various concentrations of NtpF were overlaid on NtpE immobilized on a sensor chip, a specific binding response between these subunits was observed (Fig. 4*A*). An association rate constant, $k_{on} = 2.3 \times 10^4\ M^{-1}s^{-1}$, and a dissociation rate constant, $k_{off} = 4.8 \times 10^{-4}\ s^{-1}$, were obtained. The consequent dissociation constant of K_D (k_{off}/k_{on}) was 2.1×10^{-8} M. As shown in Fig. 4 (*B* and *C*), the immobilized NtpI^{Nterm} bound both NtpF and NtpEF complex. NtpF binding to NtpI^{Nterm} was extremely fast, reaching equilibrium immediately after NtpF injection, and the complex dissociated as soon as the flow solution was switched to a running buffer (Fig. 4*B*). Therefore, it was difficult to calculate the kinetic parameters (k_{on} and k_{off}) directly. The affinity of the interaction was determined from the level of binding at equilibrium as a function of the sample concentrations; equilibrium dissociation constant (K_D) = 1.9×10^{-5} M. When various concentrations of purified NtpE-F complex were added to immobilized NtpI^{Nterm}, $k_{on} = 2.2 \times 10^5\ M^{-1}s^{-1}$ and $k_{off} = 3.3 \times 10^{-2}\ s^{-1}$ were obtained. The dissociation constant of K_D (k_{off}/k_{on}) = 1.5×10^{-7} M. The equilibrium dissociation constant ($K_D = 1.9 \times 10^{-7}$ M) was also obtained (Fig. 4*C*), consistent with the K_D value calculated from k_{off}/k_{on}. Thus, the interaction affinity of NtpI^{Nterm}-NtpEF complex was 100-fold higher than that of NtpI^{Nterm}-NtpF.

Monodispersity and Stoichiometry of Purified Samples and Subunit-Subunit Interactions Demonstrated by AUC—Sedimentation velocity (AUC/SV) provides information about the hydrodynamic property of a sample and establishes the size distribution of proteins due to their different rates of migration in the centrifugal field depending on their masses and shapes (37). Sedimentation equilibrium (AUC/SE) is suitable for determination of the weight-average molecular mass and for the study of protein self-association (38). Fig. 5 shows the continuous distribution c(s) *versus* observed sedimentation coefficient of the samples by AUC/SV, the apparent molecular masses determined by AUC/SE using a simple monomeric analysis model, and $s_{20,w}$ values calculated from the weight average sedimentation coefficient of the c(s) peak. The $s_{20,w}$ values were much larger than the observed *s* values owing to the high viscosity of the D buffer containing 10% glycerol. The c(s) distribution of purified NtpE showed a single broad peak (Fig. 5*A*). By

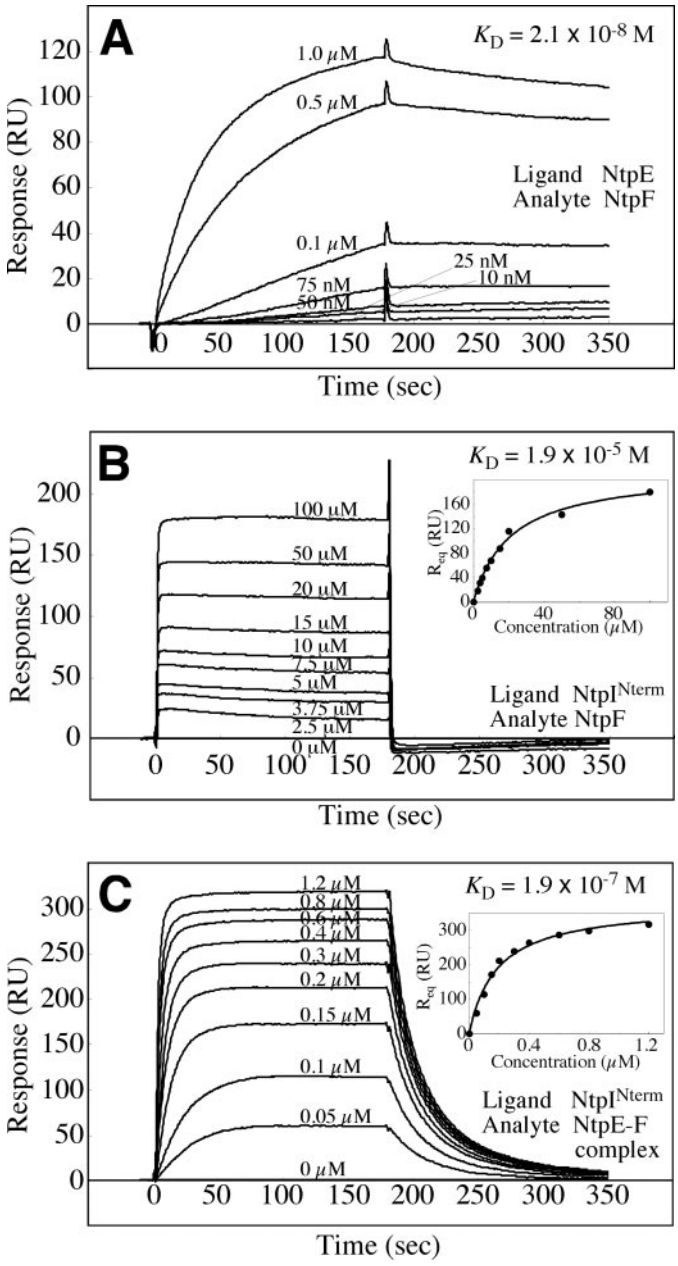

FIGURE 4. **Real-time binding measurement by BIAcore system.** Sensorgrams for the binding of various concentrations of the analyte to ligand are shown. The responses on the sensorgrams are designated in resonance units (RU). The *inset* shows the kinetic plot and binding isotherm for binding of NtpF or the NtpE-F complex to the NtpI^{Nterm} sensor chip at various protein concentrations. The fitted curve and the K_D values were obtained using the BIAevaluation software with a single 1:1 interaction binding isotherm. *A*, interaction of NtpE and NtpF. *B*, interaction of NtpI^{Nterm} and NtpF. *C*, interaction of NtpI^{Nterm} and NtpE-F complex.

increasing the protein concentrations (0.2, 0.4, and 0.8 mg of protein/ml), the weight averages of the peak increased (1.40, 1.41, and 1.48 S, respectively; data for 0.2 and 0.4 mg of protein/ml were not shown). The apparent molecular mass determined by AUC/SE was 34.6 ± 0.2 kDa, which was greater than the theoretical value (23 kDa) based on the amino acid sequence. These findings suggested that the NtpE exists in a relatively rapid equilibrium between the monomer-dimer (or oligomer) species. We applied several models for fitting the AUC/SE data. The monomer-dimer equilibrium model using

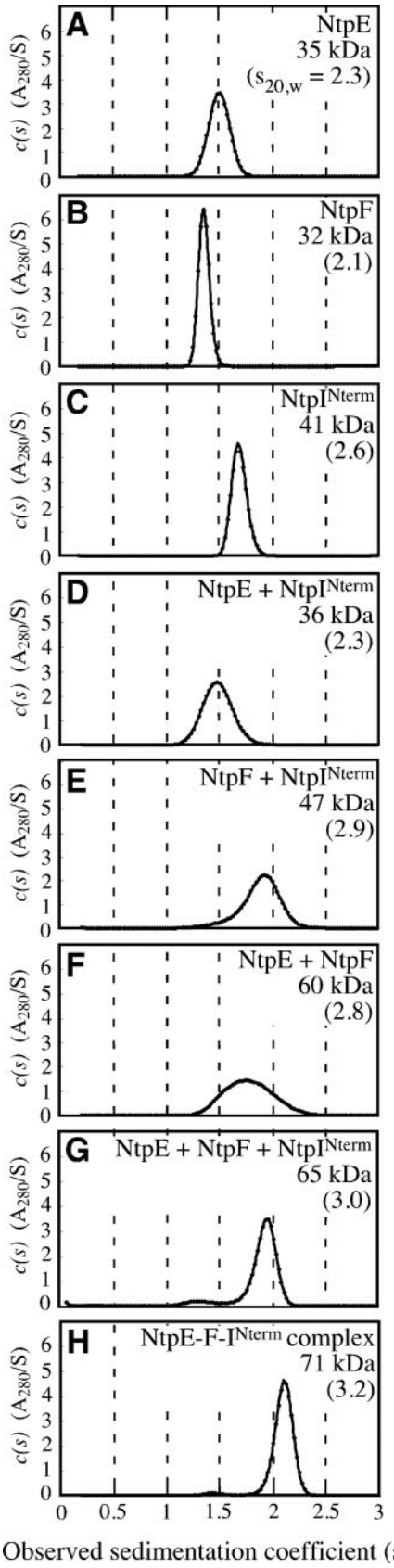

FIGURE 5. **Distribution of sedimentation coefficients c(s) for purified subunits, mixed samples and purified NtpE-F-I^{Nterm} complex by AUC/SV experiments.** Calculated c(s) at 0.8 mg/ml sample is plotted *versus* observed sedimentation coefficient (s). Each figure (*A–H*) shows sample name, apparent molecular mass of the sample, which was determined by AUC/SE experiments using a simple monomeric analysis model, and the $s_{20,w}$ value (sedimentation coefficient corrected to 20 °C in pure water) in parenthesis calculated from the observed sedimentation coefficient value of the c(s) peak.

the theoretical molecular mass (23 kDa) gave a good global fit and an equilibrium constant of $2.4 \pm 0.1 \times 10^{-5}$ M was estimated. The c(s) distribution of purified NtpF showed a single prominent peak (Fig. 5*B*). By increasing the protein concentrations (0.2, 0.4, and 0.8 mg/ml), the weight averages of the peak were constant (1.37, 1.37, and 1.36 S, respectively; data for 0.2 and 0.4 mg/ml not shown). The apparent molecular mass was 31.6 ± 0.2 kDa, which agreed well with that of the dimer (theoretical value for NtpF; 15 kDa). These findings suggested that the NtpF exists as a dimer in the protein concentration range (0.2–0.8 mg/ml). The c(s) distribution of purified NtpI^{Nterm} showed a single prominent peak (Fig. 5*C*). The weight averages of the peak remained constant (1.70, 1.68, and 1.69 S) at different protein concentrations (0.2, 0.4, and 0.8 mg/ml respectively; data for 0.2 and 0.4 mg/ml not shown). The apparent molecular mass was 41.0 ± 0.1 kDa, which agreed well with the theoretical value (40 kDa). These findings suggested that the NtpI^{Nterm} exists as a monomer in the protein concentration range (0.2–0.8 mg/ml).

Subunit-subunit interactions were analyzed from the increase of the sedimentation coefficients of mixed samples compared with those of independent subunits. The c(s) distribution peak (at 1.49 S) of the mixed sample at molar ratio 1:1 (NtpE dimer:NtpI^{Nterm} monomer) did not change much compared with that of NtpE (at 1.48 S) or NtpI^{Nterm} (at 1.69 S) (Fig. 5*D*). The apparent molecular mass (36 kDa) was close to that of NtpE (35 kDa) or NtpI^{Nterm} (41 kDa). These findings suggest that NtpE does not interact with NtpI^{Nterm}, consistent with the results of pulldown experiments as described above. Mixed samples at the molar ratio 1:1 (:1) (NtpF dimer:NtpI^{Nterm} monomer, NtpE dimer:NtpF dimer, and NtpI^{Nterm} monomer:NtpE dimer:NtpF dimer) were also examined by AUC (Fig. 5, *E–G*). The sedimentation coefficients (1.90, 1.79, and 1.93 S, respectively) and apparent molecular masses obtained (47, 60, and 65 kDa, respectively) were clearly larger than those of any one of the subunits. Thus, the suggested interactions between NtpF-NtpI^{Nterm}, NtpE-NtpF, and NtpE-NtpF-NtpI^{Nterm} were confirmed.

Monodispersity and the molecular mass of the purified NtpE-F-I^{Nterm} complex were analyzed by AUC. The sedimentation velocity experiments for the purified NtpE-F-I^{Nterm} complex were conducted at a concentration of 0.8 mg/ml. The resulting c(s) distribution of the complex showed the presence of a well defined peak with a sedimentation coefficient of 2.09 S (95% of the total fraction) and a minor broad peak with 1.31 S (<3% of the total) (Fig. 5*H*). The weight average f/f_o value was optimized by least-squares regression and converged to a best-fit value of 2.02. The molecular mass calculated from these results was 81.7 kDa, which corresponds to that of a 1:1:1 ternary complex (78 kDa). The apparent molecular mass of the complex by AUC/SE, 70.9 ± 0.4 kDa, is smaller than the predicted 78 kDa because of the slow dissociation of the complex at the protein concentrations tested (0.15, 0.2, and 0.4 mg/ml).

These findings suggest that the ternary complex is formed with 1:1:1 stoichiometry.

SAXS Measurement of Purified NtpE-F-I^{Nterm} Complex—Fig. 6*A* shows the SAXS profiles of the NtpE-F-I^{Nterm} complex and associated Guinier plots (shown in *inset*). The Guinier plots at three different concentrations (1.7, 2.4, and 3.0 mg/ml) presented single regression lines, suggesting monodispersive properties and no aggregation effect of the NtpE-F-I^{Nterm} complex in the concentration range. The normalized forward scattering intensity $I(0, c)$ and apparent radius of gyration $R_g(c)$ are also constants in the concentration range (1.7–3.0 mg/ml) as shown in Fig. 6*B*. $I(0, 0)$ and $R_g(0)$, which were determined by extrapolation of the dependence to infinite diluted condition ($c = 0$) were 9.92 ± 1.18 and 7.05 ± 0.11 nm, respectively. The pair distribution function, $P(r)$, calculated by applying the SAXS profiles without the data points in $q < 0.1072$ nm^{-1}, suggested an elongated molecular shape with a maximum molecular length (D_{max}) of 23.0 nm (Fig. 6*C*). Comparison of the forward scattering with the value obtained from a reference solution of bovine serum albumin indicated a molecular mass of 73.2 ± 8.7 kDa. The estimated value is similar to the theoretical molecular mass (78 kDa) of the complex calculated from the amino acid sequence for the 1:1:1 ternary complex. SDS-PAGE analysis revealed the NtpE-F-I^{Nterm} complex contained three clear protein bands (Fig. 2*B*, *lane 6*). In addition the complex sample was monodisperse. Therefore, we concluded that the NtpE-F-I^{Nterm} complex is formed with 1:1:1 stoichiometry.

The low resolution model of the NtpE-F-I^{Nterm} complex was reconstructed by DAMMIN. The shape obtained for the NtpE-F-I^{Nterm} complex is a good fit to the experimental data in the entire scattering range. All ten independent reconstructions showed a similar elongated "L" shape and have been averaged as shown in Fig. 7*A*. The complex appears as an "L"-shaped molecule of ~16 nm in length.

DISCUSSION

In this study, we purified NtpE, NtpF, and NtpI^{Nterm} individually and showed that these three subunits make up a complex with a 1:1:1 stoichiometry. Does the resulting NtpE-F-I^{Nterm} complex function as a structural element in the intact *E. hirae* V-ATPase? Previously, we have established a purification and reconstitution system for whole *E. hirae* V_1V_o-ATPase (20). Addition of EDTA to chelate the Mg^{2+} results in dissociation of the V_1 moiety from reconstituted V_1V_o-proteoliposomes. Reincubation of the dissociated V_1 fraction with V_o-liposomes in the presence of Mg^{2+} resulted in a full recovery of the Na^+-stimulated ATPase activity and Na^+-transporting activity, suggesting that dissociation did not cause inactivation of either the V_1 or V_o moieties of the V-ATPase (20). The dissociated V_1 fraction contained two subcomplexes (the NtpE-F complex and the $NtpA_3$-B_3-D-G complex retaining ATP hydrolytic activity) and NtpC, which were separated by anion-exchange and gel-filtration column chromatography.[3] Based on the results of *Thermus thermophilus* V-ATPase studies (39), NtpC seems to be located between the $NtpA_3$-B_3-D-G complex and the NtpK ring in the V-ATPase (33). Therefore, the NtpE-F complex is likely to comprise the peripheral stalk together with the N-terminal hydrophilic domain of NtpI (stator membrane subunit) (Fig. 1), consistent with the findings in this study.

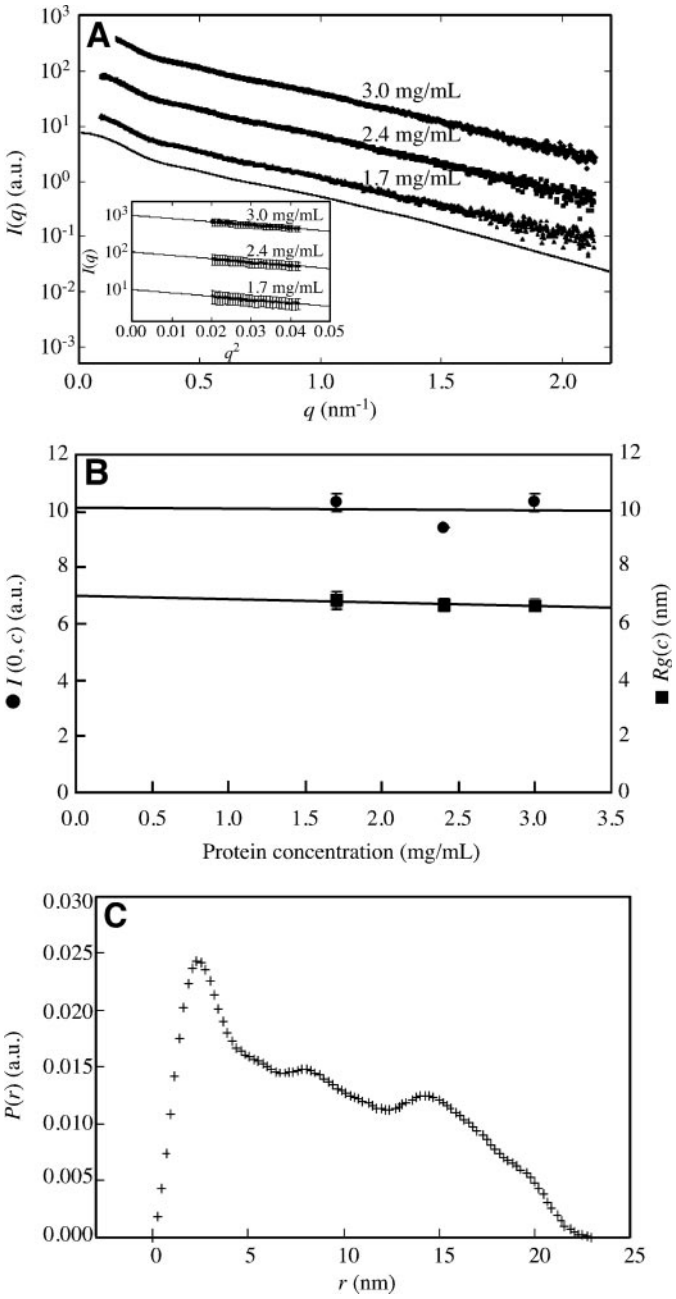

FIGURE 6. **SAXS profiles of the NtpE-F-I^{Nterm} complex.** *A*, scattering profiles and corresponding Guinier plots. The scattering profiles at protein concentrations of 3.0 (*filled circle*), 2.4 (*filled square*), and 1.7 mg/ml (*filled triangle*) are plotted in semilogarithmic form and shifted appropriately along the ordinate for clarity. The *solid line* shows the calculated profile from the structural model reconstructed by DAMMIN. In the *inset*, the least-squares fit of Equation 1 to the q range satisfying the criteria for the Guinier approximation $q_{max}R_g(c) < 1.3$ are shown as *solid lines*. All plots are offset for the sake of clarity. *B*, the concentration dependence of forward scattering at zero degree and the apparent radius of gyrations. The apparent radius of gyrations, $R_g(c)$, and forward scattering intensity, $I(0, c)$, normalized by the concentration are plotted. The least-squares fitting and extrapolations to the infinite diluted condition are shown. *C*, the pair distribution $P(r)$ function of NtpE-F-I^{Nterm} complex calculated by GNOM is shown.

AUC experiments showed that purified NtpI^{Nterm} is stable as a monomer in solution (Fig. 5*C*), whereas purified NtpE exists

[3] T. Murata, unpublished data.

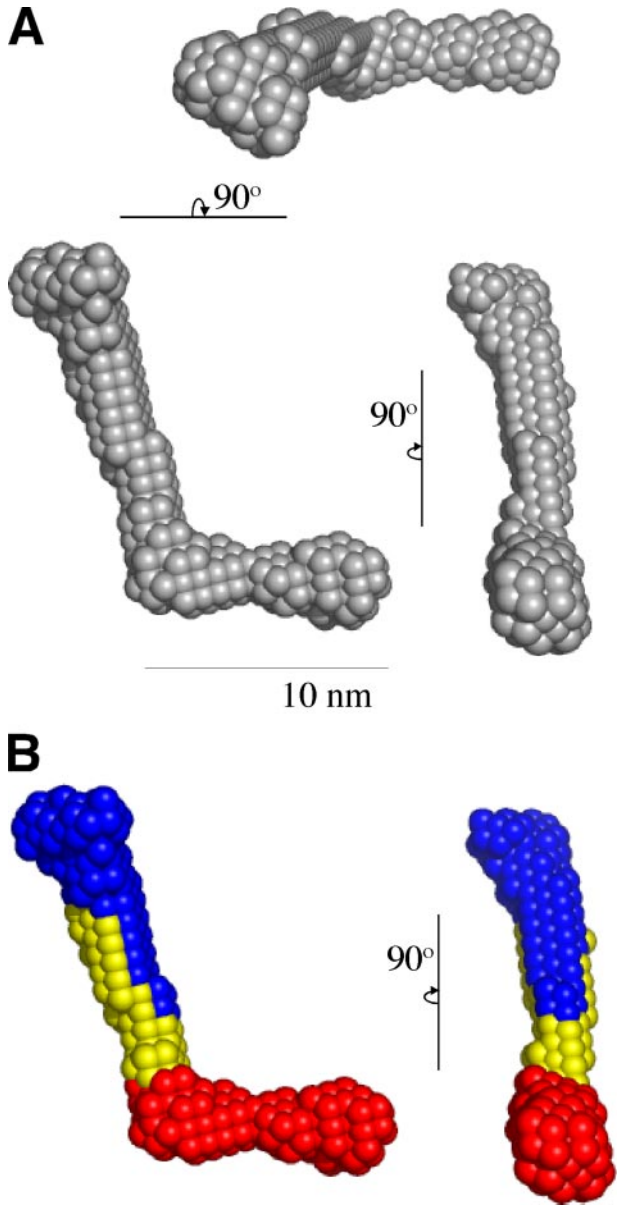

FIGURE 7. **Low resolution structure model of NtpE-F-I^{Nterm} complex determined from SAXS data.** *A*, the molecular model of NtpE-F-I^{Nterm} complex was reconstructed by DAMMIN and DAMAVER. *B*, imaginary illustration of subunits arrangement fitted to the molecular model. NtpE, NtpF, and NtpI^{Nterm} are colored in *blue*, *yellow*, and *red*, respectively.

in a monomer-dimer (or oligomer) equilibrium (Fig. 5*A*) and purified NtpF forms a dimer in solution (Fig. 5*B*). It is not clear how dimers of NtpF and NtpE dissociate into monomers for formation of the 1:1:1 NtpE-F-I^{Nterm} complex. CD spectroscopy experiments showed that, upon NtpE-F complex formation, there was an increase in α-helical secondary structure, most likely due to α-helical coiled-coil formation between the two subunits as indicated by stronger minima at 208 and 222 nm and by the increased ratio of $\theta_{222}/\theta_{208}$. The dissociation of the respective dimer of each subunit is likely to take place during formation of the interaction between NtpE and NtpF, as shown for studies on other V (or A)-ATPases (8, 36).

The observed K_D values estimated by surface plasmon resonance assay were calculated for all monomers in solution using evaluation software with a single 1:1 interaction binding isotherm. However, isolated NtpE and NtpF exist as oligomers in solution as described above. The observed K_D values must vary depending on the oligomeric states of the subunits. In contrast the dissociation rate constants (k_{off}) should not be dependent on the oligomeric states of the samples. The dissociation rate for the NtpI^{Nterm}-NtpF interaction was too rapid to be estimated (Fig. 4*B*). The dissociation rate for the NtpI^{Nterm}-NtpEF complex interaction was much slower ($k_{off} = 3.3 \times 10^{-2}$ s^{-1}) than that of the NtpI^{Nterm}-NtpF complex. In addition, the purified NtpE-F-I^{Nterm} complex was monodisperse in solution as observed by AUC and SAXS. Thus, the interaction affinity of NtpI^{Nterm}-NtpEF complex is concluded to be much higher than that of NtpI^{Nterm}-NtpF. Although direct interaction between NtpE and NtpI^{Nerm} was not observed by pulldown assay (Fig. 2*B*, *lane 3*) and AUC (Fig. 5*D*), NtpE seems to help increase the binding affinity of NtpI^{Nterm} and NtpF.

The structure model of the NtpE-F-I^{Nterm} ternary complex obtained by SAXS revealed an elongated L-shape (Fig. 7*A*). Electron microscopic analysis of the EG complex of yeast V-ATPase with a 1:1 stoichiometry indicated a rod shape (8). Therefore, we can speculate that the NtpE-F complex corresponds to the *blue* and *yellow parts* in the L-shaped structure shown in Fig. 7*B*. Therefore, the remaining region shown in *red* is likely to correspond to the NtpI^{Nterm}. CD analysis implied that NtpE and NtpF interact through α-helical coiled-coil formation (Fig. 3). The pulldown assay using one tagged subunit and AUC experiments show that NtpI^{Nterm} binds NtpF directly but not NtpE (Fig. 2*B*, *lane 5*). From these findings, we predict that NtpE and NtpF correspond to the *blue* and *yellow regions* in the L-shaped structure, respectively.

Most recently, analysis by mass spectrometry has indicated that there are three peripheral stalks (EG heterodimer) in yeast V-ATPase (11). In contrast, there are two EG heterodimers in the *T. thermophilus* enzyme (12), consistent with the electron microscopy images (40). In this study, we demonstrate that a single NtpE-F heterodimer of *E. hirae* V-ATPase binds to the N-terminal hydrophilic domain of NtpI (1–341 residues).

Acknowledgments—We thank Drs. Masaki Yamamoto, Naoto Yagi, Mamoru Sato, and Sam-Yong Park for helpful advice and coordination for SAXS experiments. We also thank Sayaka Tojo, Mieko Ueno, Naoko Shinya, Tomoko Inoue, Keiko Honda, and Ryogo Akasaka for technical support of initial expression trials and CD spectroscopy experiment, and Dr. Bernadette Byrne for critical reading of the manuscript. The synchrotron radiation experiments were performed at the beamline BL45XU at SPring-8 with the approval of the RIKEN SPring-8 Center (Proposal 20070167).

REFERENCES

1. Forgac, M. (2007) *Nat. Rev. Mol. Cell. Biol.* **8,** 917–929
2. Sumner, J. P., Dow, J. A., Earley, F. G., Klein, U., Jager, D., and Wieczorek, H. (1995) *J. Biol. Chem.* **270,** 5649–5653
3. Kane, P. M., and Smardon, A. M. (2003) *J. Bioenerg. Biomembr.* **35,** 313–321
4. Jones, R. P., Durose, L. J., Findlay, J. B., and Harrison, M. A. (2005) *Biochemistry* **44,** 3933–3941
5. Landolt-Marticorena, C., Williams, K. M., Correa, J., Chen, W., and Manolson, M. F. (2000) *J. Biol. Chem.* **275,** 15449–15457

6. Inoue, T., and Forgac, M. (2005) *J. Biol. Chem.* **280,** 27896–27903
7. Norgett, E. E., Borthwick, K. J., Al-Lamki, R. S., Su, Y., Smith, A. N., and Karet, F. E. (2007) *J. Biol. Chem.* **282,** 14421–14427
8. Fethiere, J., Venzke, D., Diepholz, M., Seybert, A., Geerlof, A., Gentzel, M., Wilm, M., and Bottcher, B. (2004) *J. Biol. Chem.* **279,** 40670–40676
9. Fethiere, J., Venzke, D., Madden, D. R., and Bottcher, B. (2005) *Biochemistry* **44,** 15906–15914
10. Ohira, M., Smardon, A. M., Charsky, C. M., Liu, J., Tarsio, M., and Kane, P. M. (2006) *J. Biol. Chem.* **281,** 22752–22760
11. Kitagawa, N., Mazon, H., Heck, A. J., and Wilkens, S. (2008) *J. Biol. Chem.* **283,** 3329–3337
12. Esteban, O., Bernal, R. A., Donohoe, M., Videler, H., Sharon, M., Robinson, C. V., and Stock, D. (2008) *J. Biol. Chem.* **283,** 2595–2603
13. Yokoyama, K., and Imamura, H. (2005) *J. Bioenerg. Biomembr.* **37,** 405–410
14. Murata, T., Yamato, I., and Kakinuma, Y. (2005) *J. Bioenerg. Biomembr.* **37,** 411–413
15. Lolkema, J. S., Chaban, Y., and Boekema, E. J. (2003) *J. Bioenerg. Biomembr.* **35,** 323–335
16. Murata, T., Igarashi, K., Kakinuma, Y., and Yamato, I. (2000) *J. Biol. Chem.* **275,** 13415–13419
17. Murata, T., Kakinuma, Y., and Yamato, I. (2001) *J. Biol. Chem.* **276,** 48337–48340
18. Murata, T., Kawano, M., Igarashi, K., Yamato, I., and Kakinuma, Y. (2001) *Biochim. Biophys. Acta* **1505,** 75–81
19. Murata, T., Takase, K., Yamato, I., Igarashi, K., and Kakinuma, Y. (1997) *J. Biol. Chem.* **272,** 24885–24890
20. Murata, T., Takase, K., Yamato, I., Igarashi, K., and Kakinuma, Y. (1999) *J. Biochem.* (*Tokyo*) **125,** 414–421
21. Kakinuma, Y., Yamato, I., and Murata, T. (1999) *J. Bioenerg. Biomembr.* **31,** 7–14
22. Keenan Curtis, K., and Kane, P. M. (2002) *J. Biol. Chem.* **277,** 2716–2724
23. Horton, R. M., Hunt, H. D., Ho, S. N., Pullen, J. K., and Pease, L. R. (1989) *Gene* (*Amst.*) **77,** 61–68
24. Kigawa, T., Yabuki, T., Matsuda, N., Matsuda, T., Nakajima, R., Tanaka, A., and Yokoyama, S. (2004) *J. Struct. Funct. Genomics* **5,** 63–68
25. Laue, T. M., Shah, B. D., Ridgeway, T. M., and Pelletier, S. L. (1992) *Analytical Ultracentrifrugation in Biochemistry and Polymer Science*, pp. 19–125. Royal Society of Chemistry, Cambridge, UK
26. Schuck, P., Perugini, M. A., Gonzales, N. R., Howlett, G. J., and Schubert, D. (2002) *Biophys. J.* **82,** 1096–1111
27. Schuck, P. (2000) *Biophys. J.* **78,** 1606–1619
28. Fujisawa, T., Inoue, K., Oka, T., Iwamoto, H., Uraga, T., Kumasaka, T., Inoko, Y., Yagi, N., Yamamoto, M., and Ueki, T. (2000) *J. Appl. Crystallogr.* **33,** 797–800
29. Svergun, D. I. (1992) *J. Appl. Crystallogr.* **25,** 495–503
30. Svergun, D. I. (1999) *Biophys. J.* **76,** 2879–2886
31. Volkov, M. V., and Svergun, D. I. (2003) *J. Appl. Crystallogr.* **36,** 860–864
32. Laemmli, U. K. (1970) *Nature* **227,** 680–685
33. Murata, T., Yamato, I., Kakinuma, Y., Leslie, A. G., and Walker, J. E. (2005) *Science* **308,** 654–659
34. Kawano, M., Igarashi, K., Yamato, I., and Kakinuma, Y. (2002) *J. Biol. Chem.* **277,** 24405–24410
35. Lau, S. Y., Taneja, A. K., and Hodges, R. S. (1984) *J. Biol. Chem.* **259,** 13253–13261
36. Kish-Trier, E., Briere, L. K., Dunn, S. D., and Wilkens, S. (2008) *J. Mol. Biol.* **375,** 673–685
37. Lebowitz, J., Lewis, M. S., and Schuck, P. (2002) *Protein Sci.* **11,** 2067–2079
38. Laue, T. M., and Stafford, W. F., 3rd. (1999) *Annu. Rev. Biophys. Biomol. Struct.* **28,** 75–100
39. Iwata, M., Imamura, H., Stambouli, E., Ikeda, C., Tamakoshi, M., Nagata, K., Makyio, H., Hankamer, B., Barber, J., Yoshida, M., Yokoyama, K., and Iwata, S. (2004) *Proc. Natl. Acad. Sci. U. S. A.* **101,** 59–64
40. Bernal, R. A., and Stock, D. (2004) *Structure* **12,** 1789–1798